Journal of the American College of Cardiology Vol. 47, No. 2, 2006

Published by Elsevier Inc.

ISSN 0735-1097/06/$32.00
doi:10.1016/j.jacc.2005.07.070

Characterization of Radiofrequency Ablation Lesions With Gadolinium-Enhanced Cardiovascular Magnetic Resonance Imaging

Timm Dickfeld, MD, PHD, Ritsushi Kato, MD, PHD, Menekhem Zviman, PHD, Shenghan Lai, PHD, Glenn Meininger, MD, Albert C. Lardo, PHD, Ariel Roguin, MD, PHD, David Blumke, MD, PHD, Ronald Berger, MD, PHD, Hugh Calkins, MD, Henry Halperin, MD, MA

Baltimore, Maryland

OBJECTIVES This study was designed to evaluate the characteristics of gadolinium-enhanced imaging of radiofrequency ablations.

BACKGROUND Gadolinium-enhanced magnetic resonance imaging (MRI) has been used successfully to evaluate tissue necrosis after myocardial infarction. In electrophysiology, radiofrequency energy is used to create a targeted myocardial necrosis for the treatment of various arrhythmias.

METHODS Using a power-controlled, cooled-tip 7-F catheter system, radiofrequency lesions (10 to 40 W for 30 s) were created on the epicardium of the right ventricle in eight mongrel dogs. After injection of 0.225 mmol/kg gadolinium, T1-weighted fast gradient echo images were obtained during a follow-up of 10 h using an intrathoracic high-resolution coil. Radiofrequency ablations were analyzed on the MR images and compared with gross anatomy and histopathology.

RESULTS Four distinct phases of signal enhancement were observed. After gadolinium injection, radiofrequency lesions were delineated clearly as contrast-free areas of low signal intensity (contrast-to-noise ratio [CNR] = -21.1 ± 19.8). Signal enhancement in the lesion periphery started 4.0 ± 1.8 min after injection and progressively extended toward the lesion center at a rate of 0.02 mm/min. Full delayed enhancement was observed after 98 ± 21 min (CNR = $+17.8 \pm 9.0$). During the follow-up period, CNR started to decrease, but the lesions were detectable for as long as 10 h of follow-up. During the first three phases of enhancement, MRI correlated well with the pathological findings ($r = 0.88$, $r = 0.88$, and $r = 0.86$ [$p < 0.001$], respectively).

CONCLUSIONS Radiofrequency ablation can be evaluated accurately by using gadolinium-enhanced MRI, which may allow the noninvasive assessment of procedural success. The dissimilar wash-in and wash-out kinetics compared with myocardial infarction suggest a different pathophysiological process with complete loss of microvasculature. (J Am Coll Cardiol 2006;47: 370–8) © 2006 by the American College of Cardiology Foundation

Radiofrequency ablation (RFA) allows the catheter-based creation of well-defined, limited myocardial necrosis and has significantly changed the treatment of arrhythmias since its introduction to electrophysiology (1). However, newer ablation strategies increasingly rely on anatomic rather than electrophysiological approaches (2,3), which makes the visualization of the lesions with respect to their extent and anatomic location increasingly important. Yet, the current catheter guiding techniques mostly rely on fluoroscopy and three-dimensional mapping devices, which are limited in their ability to confirm the presence, exact location, and extent of ablation lesions, parameters that serve as indicators of the procedural success (3,4).

This anatomic information could potentially be provided by gadolinium-enhanced magnetic resonance imaging (MRI), as it has been shown to reliably visualize necrotic tissue (after myocardial infarction) with a reproducible enhancement pattern (5). First-pass images performed immediately after a gadolinium injection frequently demonstrates areas of hypoenhancement in the endocardial core of the infarct (6,7), followed by complete delayed enhancement of the myocardial necrosis 5 to 25 min after contrast injection with a subsequent wash-out period (6,8).

Correspondingly, MRI can detect the heat-related changes of T1 and T2 parameters in the necrotic myocardium after RFA and is able to confirm the existence of RFAs in the very acute setting (9). However, many clinical relevant questions, such as the characterization of radiofrequency lesions during the different stages of enhancement, the effect of radiofrequency energy on lesion visualization, and the ability to assess anatomic correlates to ablation success such as transmural extent and lesion gaps, will have to be clarified before this technology can be applied for prolonged and frequently complicated clinical procedures. Therefore, this study sought to systematically evaluate the characteristics of MRI for radiofrequency lesions.

From the Division of Cardiology, Department of Radiology, Johns Hopkins School of Medicine, and the Division of Cardiology, University of Maryland, Baltimore, Maryland.
This work has been supported by a grant of the AHA and the NHLBI (HL64795).

Manuscript received November 16, 2004; revised manuscript received June 14, 2005, accepted July 26, 2005.

METHODS

Animal preparation. Eight mongrel dogs weighting 30 to 35 kg were premedicated with 10 mg of ketamine intramus-

Abbreviations and Acronyms

ANOVA = analysis of variance
CNR = contrast-to-noise ratio
GEE = generalized estimating equation
MRI = magnetic resonance imaging
RFA = radiofrequency ablation
SI = signal intensity
SNR = signal-to-noise ratio

cularly and maintained on 80% oxygen and 1.5% isoflurane gas using a Narkomed Anesthesia ventilator (Draegar, Telford, Pennsylvania). Surface electrocardiogram leads I, II, and III were monitored continuously. Using the cutdown technique, an 8-F introducer sheath was placed in the right jugular vein for the administration of fluids and medication. Using clinical-grade surgical equipment, a thoracotomy was performed in the midsternal line and the pericardium removed. Using a standard 7-F ablation catheter with a 4-mm electrode single, radiofrequency lesions were created on the epicardial surface of the right ventricle with a clinical-grade radiofrequency generator (Atakr, Medtronic, Minneapolis, Minnesota) while the ablation site was constantly irrigated with 0.9% normal saline (21° C) at a rate of 5 ml/min. Ablation lesions were created in a linear interrupted fashion using a power-controlled mode at 10, 20, 30, and 40 W for 30 s each. After the ablation, the animals were monitored hemodynamically for 10 min, surgical tools and paramagnetic materials were removed, and the live animals were transported immediately with an unclosed chest preparation to the MRI suite. All animal protocols were reviewed and approved by the Animal Care and Use Committee at the Johns Hopkins University and conformed to the guidelines published in the "Position of the American Heart Association on Research Animal Use."

Imaging protocol. The animal was placed in a 1.5-T MR scanner (Signa XL, GE, Waukesha, Wisconsin). Using a 3-inch high-resolution coil, which was placed intrathoracically on the right ventricle, the correct imaging plane of the ablation lesions was identified with standard T1- and T2-weighted scout images. Magnevist (0.225 mmol/kg; gadopentetate dimeglumine, Berlex, Monteville, New Jersey) was injected intravenously. Continuous long-axis images were obtained throughout the area of RFA with a 3-mm slice thickness every 5 to 15min during the first 3 h and every 30 to 60 min up to a duration of 15 h using a T1-weighted, inversion prepared fast gradient recall echo sequence (TR = 3.6 ms, TE = 1.7 ms, $TI_{adjusted}$ = 175 to 275 ms [to "null" normal myocardium], field of view = 18 cm, flip angle = 20°, readout bandwidth = 32 kHz, matrix 256 × 192, number of signal averages (NEX) 1, slice thickness = 3 mm). All images were visually inspected to rule out the presence of susceptibility artifacts caused by the air-tissue interface of the open chest preparation. Animals were monitored and alive during all imaging sequences.

Postmortem examination. Immediately after the imaging protocol, the animals were injected with 20 ml of a 20% solution of 2,3,5-triphenyltetrazolium chloride and sacrificed with an intravenous injection of high-molar potassium chloride solution. The hearts were excised, fixated, and sectioned through the right ventricular lesion corresponding to the tomographic MRI slices. Lesion location, morphology, width, length, and transmural extent were determined and recorded at gross examination and photographed for later comparison with the MR images. Sections from thermally damaged tissues were submitted for histological staining (Masson's trichome and hematoxylin-eosin) and analyzed under light microscopy to characterize global morphological changes.

Data analysis. Lesion character and signal intensity (SI) were measured directly from MR images and analyzed with an off-line quantitative analysis package (version 1.53; e-film, Merge Technology, Milwaukee, Wisconsin). Lesion size was determined as the maximal lesion diameter at the outer margin of the contrast void (Phase 1) or the enhanced lesion (Phase 2 to 4).

Signal-to-noise ratio (SNR) was measured as the SI of the lesion over the standard deviation (SD) of the background noise. Contrast-to-noise ratio (CNR) was determined as the SI of lesion minus the SI of the adjacent myocardium, which was then divided by the SD of the background noise. Lesion parameters at gross examination were measured independently of magnetic resonance images and compared.

Statistical analysis. Changes in lesion size and SI were analyzed during the time-course and between the various energy groups and were considered significant at a level of $p < 0.05$ in a paired t-test (analysis of variance [ANOVA]). Comparisons of ablation lesions in MRI and in pathological specimen was performed by a native analysis using linear regression and additionally by an adjusted analysis using a generalized estimating equation approach (GEE) to control for a potential cluster effect. Unless noted otherwise, results measurements are reported as arithmetic mean ± SD. We considered p values at a level of <0.05 as statistically significant.

RESULTS

Time course of radiofrequency lesion enhancement. Independent of the radiofrequency energy and the size of the ablation lesion, all radiofrequency lesions could be visualized after enhancement using gadolinium. We injected the gadolinium 2.1 ± 0.6 h after the creation of the radiofrequency lesions.

In all experiments, four characteristic phases of enhancement were observed after the administration of gadolinium. In the first phase immediately after injection, radiofrequency lesions were visible as areas of contrast void (Figs. 1A and 1B) in comparison with the enhanced, nonablated myocardium (CNR = −21.1 ± 19.8) (Fig. 2A) and blood

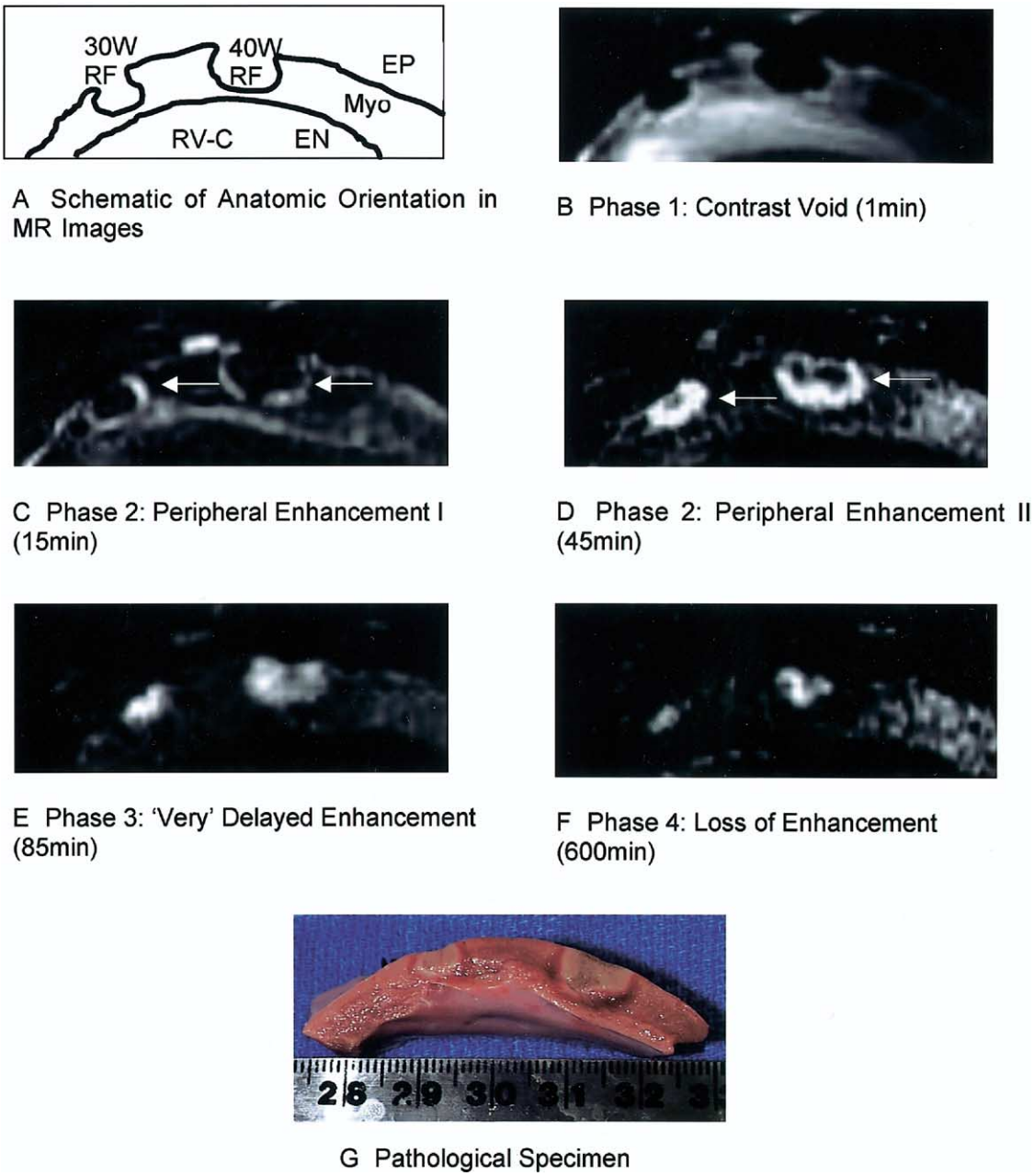

Figure 1. Gadolinium enhancement of a radiofrequency ablation lesion. The time-course (1 to 600 min) after injection of 0.225 mmol/kg gadolinium demonstrates four characteristic phases of enhancement: **(A)** Schematic of magnetic resonance (MR) images (30-W radiofrequency [RF] and 40-W RF = 30- and 40-W RF ablation lesions; Myo = right ventricular myocardial wall; EP = epicardial side; EN = endocardial side; RV-C = right ventricular cavity). **(B)** Phase 1 with a contrast void. **(C and D)** Phase 2 displaying an increasing peripheral enhancement (**white arrows**). **(E)** Phase 3 showing "very" delayed enhancement with high signal intensity throughout the ablation lesion. **(F)** Phase 4 displaying loss of enhancement with decreasing signal intensity and lesion size. **(G)** Corresponding pathological specimen.

pool (CNR = −49.8 ± 38.7). Measured SNRs were 8.1 ± 3.9 vs. 29.3 ± 17.1 ($p < 0.01$) (Fig. 2B) and 8.1 ± 3.9 vs. 59.1 ± 43.2 ($p < 0.01$), respectively. Lesion size by MRI was 7.8 ± 2.8 mm compared with in the pathological specimen 6.4 ± 2.7 mm ($p > 0.05$ for difference). Magnetic resonance imaging correlated well with pathological results ($r = 0.88$, $p < 0.001$; GEE: regression coefficient 0.87, $p < 0.0001$) (Fig. 3A) and slightly overestimated the lesion size by 1.4 ± 1.7 mm.

In the second phase, a high SI enhancement was observed starting from the lesion periphery 4.0 ± 1.8 min after injection (Figs. 1C and 1D). This ring-like enhancement increased in thickness at a rate of approximately 0.02 mm/min toward the lesion center ($r = 0.88$, $p < 0.001$; GEE correlation coefficient 0.78, $p < 0.0001$) (Fig. 3D). Peripheral hyperenhancement was well delineated against the nonenhanced lesion center (CNR = 11.5 ± 3.3; SNR 30.2 ± 14.6 vs. 18.7 ± 13.4; $p < 0.001$) and the surround-

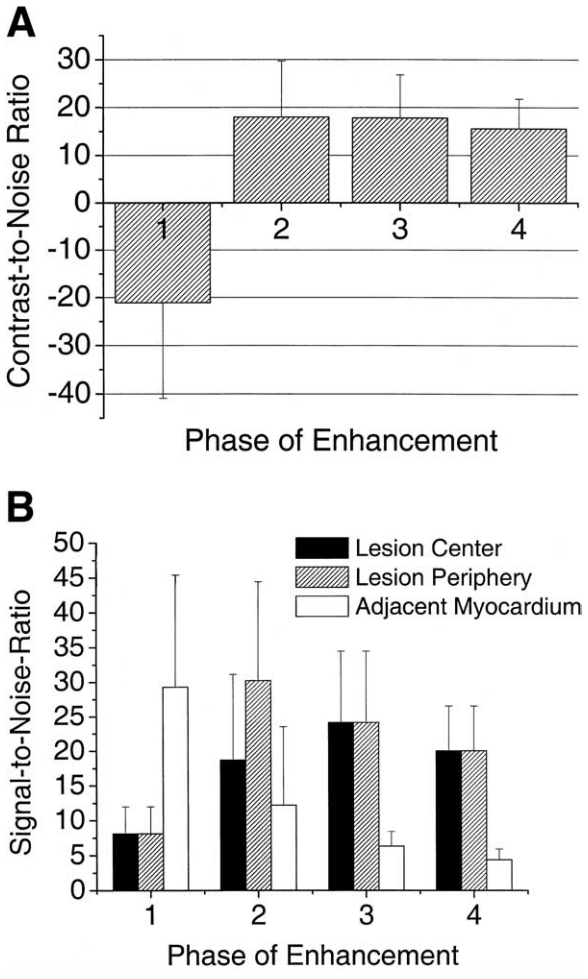

Figure 2. Contrast-to-noise-ratio during the four phases of gadolinium-enhanced imaging between the radiofrequency lesion and the adjacent myocardium **(A)**. Signal-to-noise ratio of radiofrequency lesions during the four phases of gadolinium enhancement in lesion center, lesion periphery, and adjacent myocardium **(B)**.

ing myocardium (CNR = 18.0 ± 11.7; SNR 30.2 ± 14.6 vs. 12.2 ± 11.3; $p < 0.001$) as shown (Figs. 2A and 2B). Lesion size did not differ significantly from measurement of the contrast void (Phase 1; 7.7 ± 2.6 mm vs. 7.8 ± 2.8 mm; ANOVA: $p > 0.05$) and correlated well with the pathological measurements ($r = 0.88$, $p < 0.001$; GEE regression coefficient 0.89, $p < 0.0001$) (Fig. 3B). Magnetic resonance imaging overestimated the lesion size by 1.3 ± 1.9 mm, which was not significantly different from the magnetic resonance measurements in Phase 1.

During the third phase, the complete lesions showed homogenous gadolinium enhancement (Fig. 1E). Time to complete enhancement was longer with larger lesion size and occurred in average after 98 ± 21 min (Fig. 3D). The lesion was easily detected as a result of a CNR of 17.8 ± 9.0 (SNR 24.1 ± 10.3 vs. 6.3 ± 2.1; $p < 0.0001$) (Figs. 2A and 2B) and correlated well with the pathological specimen ($r = 0.86$, $p < 0.001$; GEE regression coefficient 0.85, $p < 0.0001$) (Fig. 3C). The lesion size by MRI was 8.0 ± 3.0mm, which was not different from the lesion size estimated during the Phase 1 or 2. The magnetic resonance image overestimated the pathological lesion size by 1.6 ± 2.1mm, which was not statistically significant from Phase 1 or 2 (ANOVA).

During further follow-up, the imaged lesion size started to decrease from the periphery (Phase 4), which was matched by a beginning decrease in overall SI (Fig. 1F). After 288 ± 33 min, the CNR was 15.6 ± 6.2 (SNR 20.0 ± 6.5 vs. 4.4 ± 1.5; $p < 0.001$), which allowed the lesions to remain visible for the complete follow-up of up to 10 h (Figs. 2A and 2B). As expected, the lesion size increased with the amount of ablation energy ($p < 0.05$), but the lesion-enhancement pattern and the overall signal intensities were independent of the radiofrequency energy applied ($p > 0.05$ by ANOVA).

Assessment of transmural extent and lesion gaps. Transmural extent was assessed during the first phase of a contrast void as well as during the third phase of complete enhancement in 25 radiofrequency lesions with an average depth of 4.9 ± 1.8 mm (range, 2.0 to 10.6 mm corresponding to 26% to 100% of the ventricular wall thickness). Seven of the 25 lesions were transmural. Assessment of the transmural extension by MRI correlated well with the pathological specimen ($r = 0.87$ and $r = 0.85$, respectively, $p < 0.01$ for both; GEE regression coefficient 0.83 and 0.73, $p < 0.0001$ for both) and did not show a significant difference when analyzed for increasing degrees of transmural extent (26% to 49%, 50% to 75%, or 76% to 100%, respectively). Measurements during the phase of contrast void overestimated the transmural extent by 1.1 ± 1.3 mm and classified three nontransmural lesions incorrectly (sensitivity: 100%, specificity: 83%). During "very" delayed enhancement, the lesions appeared 1.7 ± 1.5 mm larger. One lesion was incorrectly classified as transmural and one as nontransmural (sensitivity: 86%, specificity: 95%).

Twenty-one discontinuous lesions ("gaps") with an average size of 6.0 ± 4.7 mm [range, 0 mm to 23.9 mm] were similarly assessed during the early phase of contrast void and the delayed phase of complete gadolinium enhancement (Figs. 2 and 4). Early (contrast-void) and late (complete enhancement) images after gadolinium injection allowed excellent delineation of the radiofrequency gaps with a CNR of −21.2 ± 19.6 and 17.9 ± 10.2, respectively ($p < 0.001$). The gap size was correlated well with the pathological measurements ($r = 0.86$ for both; $p < 0.01$, GEE regression coefficient 0.77 and 0.80, $p < 0.0001$ for both) and underestimated the gap by 1.3 ± 1.1 mm and 0.8 ± 1.2 mm during contrast void and complete enhancement, respectively.

Histopathology. Radiofrequency lesions were characterized by a core of severe coagulation necrosis with complete loss of cellular and vascular architecture, which covered >80% of the total lesion area. In the lesion periphery, a rim of contraction band necrosis was observed with partially intact myocardial cells and areas of intralesional hematoma. Intact vascular structures obstructed with neutrophiles,

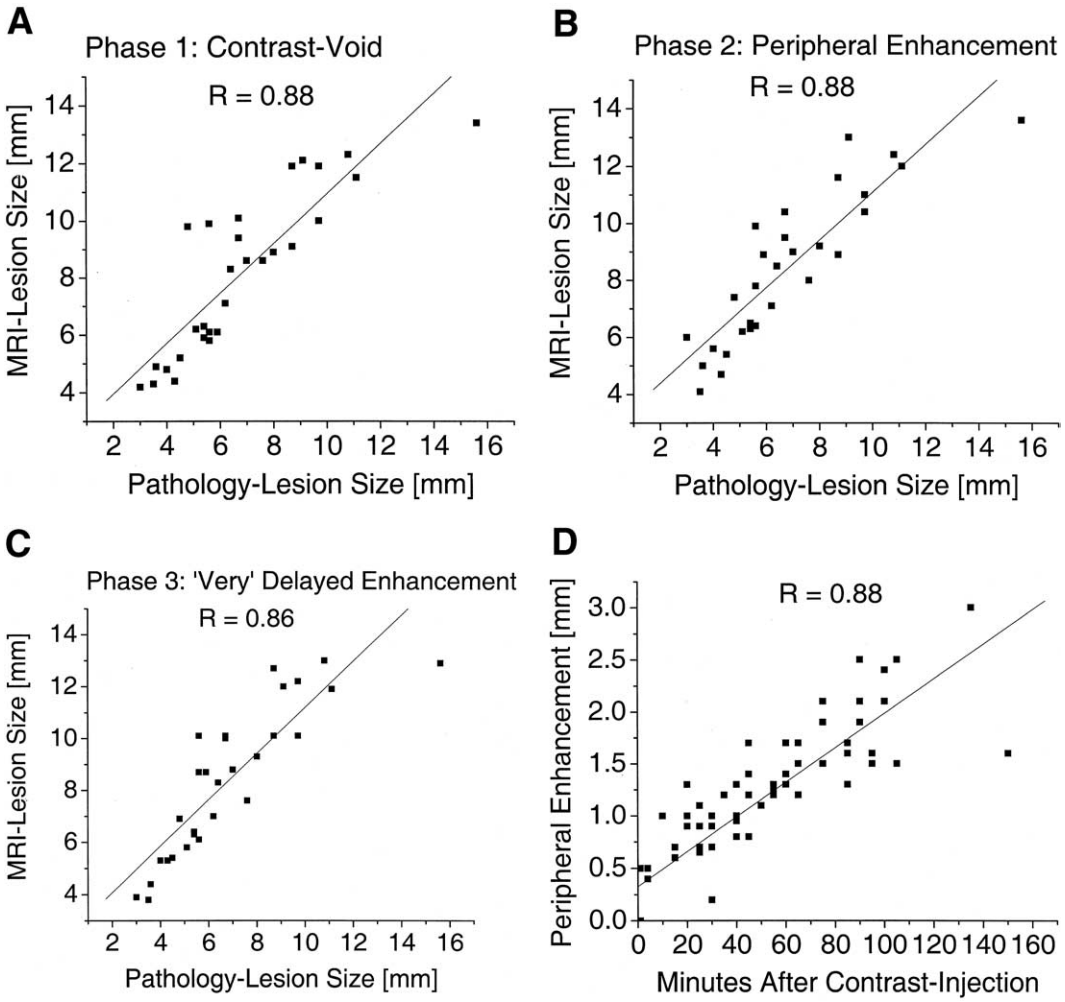

Figure 3. Correlation of radiofrequency lesion size and peripheral enhancement. Shown is the lesion size assessed in the pathological specimen compared with the lesion size assessed by magnetic resonance imaging (MRI) during the Phase 1 of contrast void **(A)**, Phase 2 of peripheral enhancement **(B)**, and Phase 3 of "very" delayed enhancement **(C)**. Increasing thickness of peripheral enhancement over time observed as a rim of high signal intensity surrounding a center of low signal after the injection of 0.225 mmol/kg of gadolinium **(D)**.

erythrocytes, and cellular fragments were observed. This area was surrounded by a perilesional rim of intact myocardial cells exhibiting edema with occasional intralesional hemorrhage, but mostly intact vasculature (Fig. 5).

DISCUSSION

Main findings. The main findings of this study are: 1) gadolinium-enhanced MRI of radiofrequency lesions displays four distinct phases of enhancement: signal void, peripheral enhancement, "very" delayed complete enhancement, and loss of enhancement; 2) radiofrequency lesions size, transmural extent, and interlesional gap can be adequately assessed throughout the different stages of gadolinium enhancement; 3) MRI appearance of radiofrequency lesions is similar over a wide range of applied energy; and 4) wash-in kinetics are different from myocardial infarction and may suggest a diffusion process.

Gadolinium enhancement of myocardial necrosis. Radiofrequency lesions of all energy levels were visible after gadolinium injection as a signal void. A lack of enhancement in the endocardial core has been described in acute myocardial infarction during the first transit of the gadolinium in only about 50% of ischemically injured segments (10) and is thought to represent occlusion of microvasculature with erythrocytes, neutrophils and cellular debris, which is also known as "no-reflow" phenomenon (6,7). However, all these segments displayed some gadolinium enhancement after about 7 min, corresponding to the near-equilibrium (pseudoequilibrium) phase with complete enhancement after about 20 min (10). Similarly, in patients undergoing ethanol-induced septal ablation for hypertrophic obstructive cardiomyopathy complete delayed enhancement could be demonstrated after 20 min (11). Differently, in RF lesions, the contrast void was a predominant characteristic after gadolinium injection in all lesions and was not replaced by complete enhancement until about 1.5 h after gadolinium was administered. This observation might be explained by the histology of the RF lesions, which showed severe

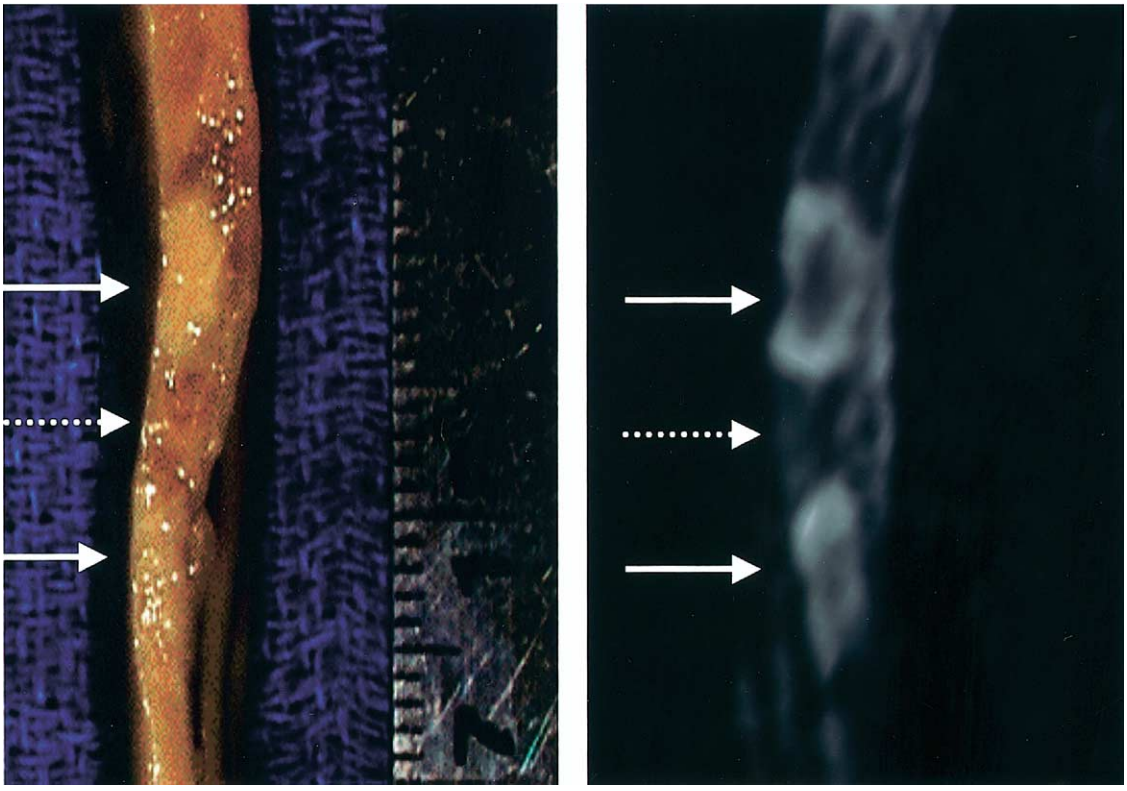

Figure 4. Evaluation of discontinuous ablation line. Gap **(dotted arrow)** observed in ablation line between two ablation lesions **(solid arrows)**. Pathological specimen after chloraldehyde preparation **(left panel)** and with gadolinium-enhanced magnetic resonance imaging **(right panel)**.

coagulation and contraction band necrosis with complete loss of cellular and vascular architecture up to a small transition zone at the periphery (12). Thus, RF lesions may exhibit an extreme and irreversible "no-reflow" phenomenon, responsible for the different wash-in kinetics observed.

These histological findings also may explain the second phase of a slowly progressive, ring-like, peripheral enhancement of RF lesions, which is different from infarcted myocardial tissue. Gadolinium with a molecular weight of approximately 800 Daltons is thought to be biologically inert and to passively diffuse throughout the extracellular space (13). Although after myocardial infarction reperfusion or collateral blood supply achieves complete delayed hyperenhancement after 10 min (6–8), enhancement of the devascularized RF lesion seems to rely mostly on diffusion from the lesion periphery. Because the diffusion time increases with the distance the lack of functional capillaries might explain the prolonged time course when compared with infarcted myocardium (14).

Thus, we suggest the term "very delayed enhancement" to describe the prolonged time course of RF lesion enhancement compared with the observations in myocardial infarction that occurs significantly earlier (5,6). Increase in volume of distribution and regional differences in wash-in/wash-out time constants have been proposed as possible mechanisms of hyperenhancement in infarcted tissue (5,15–17). An accumulation of gadolinium within the area of hyperenhancement was recently shown by Rehwald et al. (17), who demonstrated an increased gadolinium concentration of 235 ± 24% in acute infarct and of 472 ± 78% in chronic infarct measured directly with electron probe x-ray microanalysis. On the other hand, Kim et al. (5) were able to show that in 13 rabbits the differences in regional enhancement were mostly due to changes in regional microsphere-determined flow.

In our experiments, gadolinium imaging slightly overestimated the pathological lesion size (and therefore underestimated the gap size) during the different phases of delayed enhancement. Similarly, several MR studies overestimated the size of myocardial infarction by 10% to 20%, which was contributed to an increased accumulation in the border zone (7,16,18,19). However, detailed ex vivo studies using ultrathin MRI (500 μm) have demonstrated a good correlation of delayed hyperenhancement with the area of myocardial necrosis (8). Additionally, direct measurements of gadolinium in the adjacent myocardium of risk that failed to show a significant increase in gadolinium contents (17). Therefore, overestimation in lesion size of myocardial infarction and RF lesions is possibly the result of partial-volume effects caused by slice thickness requirements inherent to in vivo imaging (8).

During further follow-up, the peripheral enhancement of the RF lesions was increasingly lost ("shrinking lesion") as well as the overall signal decreased ("less bright lesion"). However, lesions remained visible for up to 10 h. Wash-out studies in myocardial infarction similarly described a periph-

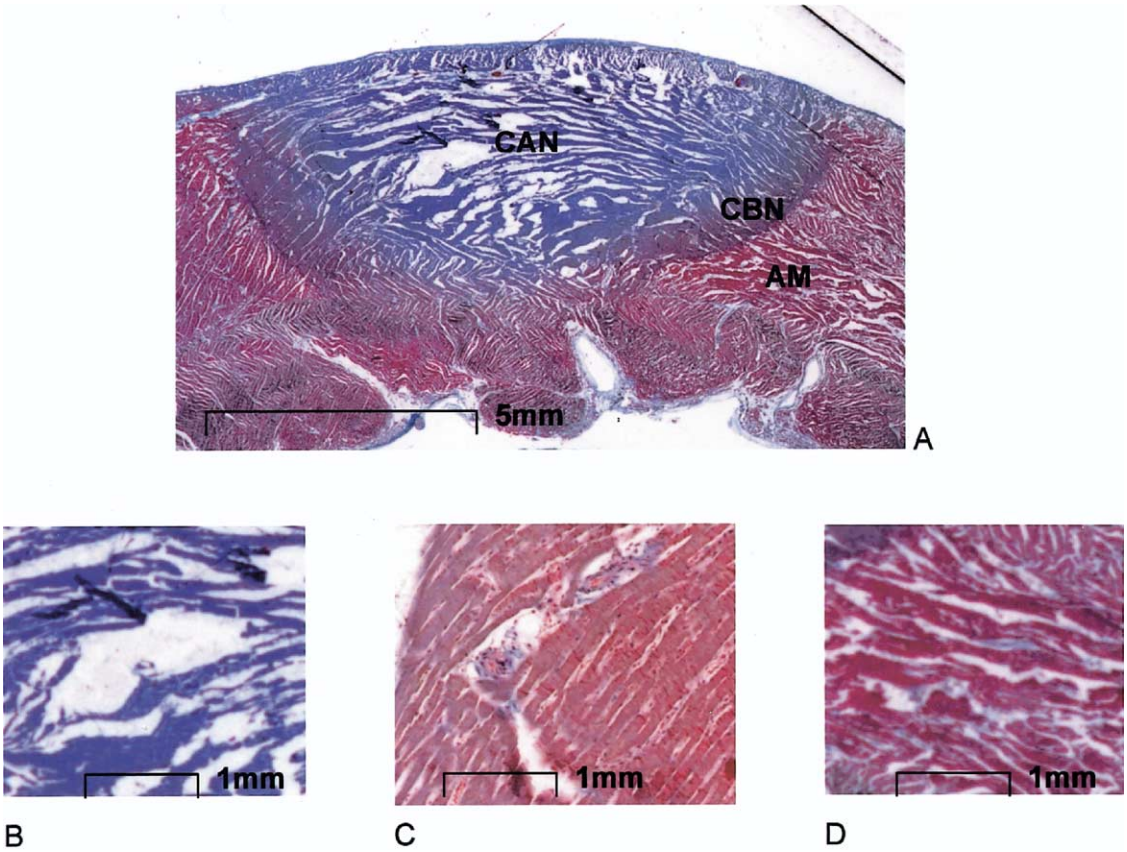

Figure 5. Radiofrequency ablation lesion. Masson's trichrome stain. **(A)** AM = adjacent myocardium; CAN = coagulation necrosis; CBN = contraction band necrosis. **(B) Blue** center core with severe coagulation necrosis, necrotic cavity, and complete loss of cellular structure. **(C) Light purple** periphery demonstrating contraction band necrosis with erythrocytes and cell debris in vasculature. **(D)** Adjacent viable myocardium. Calibration bars are presented in millimeters (mm).

eral decrease in enhancement. However, a significant loss of hyperenhanced regions except for centrally located patches has been described as early as 25 min after gadolinium injection (5). The differences in the time course can likely be attributed to the histologic changes in RF lesions, resulting in a slower diffusion-only process out of the ablated area.

Gadolinium enhancement of RFAs. Experiences with gadolinium-enhanced imaging of RF lesions have been very limited. In the only animal study Lardo et al. (9) reported a 12 min follow-up of RF lesions in the right ventricle of six mongrel dogs. He described hyperenhancement of the lesions after 1 min with an SI of 1.55 ± 0.16 times the preinjection values and gradual signal decrease during the 11 min of follow-up. These data differ from our observations and might be the result of a partial-volume effect and a difference in resolution. Although our study used a high-resolution coil with a slice thickness of 3 mm for an RF lesions size of 6.4 ± 2.7 mm, Lardo et al. (9) used a cardiac phase array with a slice thickness of 7 mm for an average lesion of only 3.4 ± 2.1 mm. This may have prohibited a more detailed evaluation of regional differences within the lesion. Additionally, a smaller lesion size may have facilitated a more rapid diffusion of gadolinium into the lesion.

The only other report is a case study showing delayed enhancement in an area of previous RFA for idiopathic left ventricular tachycardia in an 45-year-old patient (20).

Although our findings differ substantially from the observations in gadolinium-enhancement after myocardial infarction several similarities can be found with MRI of RFA in noncardiac tissue. After RFA of prostate cancer in 10 patients, lesions appeared as hypointense foci immediately after gadolinium injection (21). After ablation of liver metastasis, Goldberg and Dupuy described a lack of enhancement immediately after gadolinium injection, but a rim-like enhancement in delayed images (22). In multiple animal studies, RF lesions in liver, lung, brain, and pancreas displayed a characteristic pattern of nonenhancing center with peripheral rim enhancement (23–26). Lesion size correlated well with the pathological specimen ($r = 0.91$ to 0.93) (23) and overestimated the lesion size by 0.8 ± 1.2 mm (23) to 2.2 ± 1.0 mm (27), which may suggest that the histology changes rather than the type of tissue determine the MRI characteristics.

Study limitations. Several limitations have to be considered related to this study. Although most of the clinical RF lesions are created endocardially, epicardial lesions were chosen in this study to allow controlled lesion creation and

guarantee lesion creation over a wide variety of energy as its evaluation was on of the goals of the study. While the macroscopic and histological appearance of the ablation lesions in our study was similar to those described for endocardial ablations (12), we cannot rule out a possible effect on imaging characteristics.

Gadolinium injection and MRI was performed 2.1 ± 0.6 h after RFA. In our study, this was due to the transfer time and the necessary setup in the MRI scanner. However, clinical procedure times for complicated ablations frequently are several hours; thus, if MRI is used for postprocedural assessment, an RF lesion age of 2 h is realistic.

Histological changes occurring during the days and weeks after ablation (12) and may influence the wash-in and wash-out kinetics. In our experiments, no differences in the enhancement pattern were observed between different experiments, nor did other RF studies of longer follow-up (24). However, future studies will have to address this issue.

Clinical implications. Recent advances in ablation strategies advocate an anatomic rather than electrophysiological approach toward ablation of, e.g., isthmus-dependent flutter, atrial fibrillation, and nonidiopathic ventricular tachycardia (2,3). Although current catheter guiding techniques have only a limited ability to demonstrate the location and size of an ablation lesion, gadolinium-enhanced MRI could assess the ablation results after complex RFA and potentially provide an end point for these anatomically guided procedures. In interventional MRI/fluoroscopy units, MR images could be used to assess incremental progress during the procedure. The new generation of electrophysiologic mapping systems with image integration capability could provide images of failed ablations (e.g., gaps in ablation lines) and direct repeat procedures. Finally, with a potential real-time MRI system continuous information about the cardiac anatomy and the ablation lesions could be obtained.

This study showed that some significant differences exist between the pattern of delayed enhancement of necrotic tissue in myocardial infarction and after radiofrequency ablation. However, the knowledge about these dissimilarities may allow—as in this study—to reliably evaluate the ablation lesions throughout the different phases of enhancement. Additional studies are now warranted to further define its clinical applicability in electrophysiology and possibly open another application of MRI in the field of cardiology.

Reprint requests and correspondence: Dr. Timm Dickfeld, University of Maryland, School of Medicine, Division of Cardiology, 22 South Greene Street, Room N3W77, Baltimore, Maryland 21201. E-mail: tdickfel@medicine.umaryland.edu.

REFERENCES

1. Huang SK, Bharati S, Graham AR, Lev M, Marcus FI, Odell RC. Closed chest catheter desiccation of the atrioventricular junction using radiofrequency energy—a new method of catheter ablation. J Am Coll Cardiol 1987;9:349–58.
2. Marchlinski FE, Callans DJ, Gottlieb CD, Zado E. Linear ablation lesions for control of unmappable ventricular tachycardia in patients with ischemic and nonischemic cardiomyopathy. Circulation 2000; 101:1288–96.
3. Pappone C, Rosanio S, Oreto G, et al. Circumferential radiofrequency ablation of pulmonary vein ostia: A new anatomic approach for curing atrial fibrillation. Circulation 2000;102:2619–28.
4. Willems S, Weiss C, Ventura R, et al. Catheter ablation of atrial flutter guided by electroanatomic mapping (CARTO): a randomized comparison to the conventional approach. J Cardiovasc Electrophysiol 2000;11:1223–30.
5. Kim RJ, Chen EL, Lima JA, Judd RM. Myocardial Gd-DTPA kinetics determine MRI contrast enhancement and reflect the extent and severity of myocardial injury after acute reperfused infarction. Circulation 1996;94:3318–26.
6. Lima JA, Judd RM, Bazille A, Schulman SP, Atalar E, Zerhouni EA. Regional heterogeneity of human myocardial infarcts demonstrated by contrast-enhanced MRI. Potential mechanisms. Circulation 1995;92: 1117–25.
7. Judd RM, Lugo-Olivieri CH, Arai M, et al. Physiological basis of myocardial contrast enhancement in fast magnetic resonance images of 2-day-old reperfused canine infarcts. Circulation 1995;92:1902–10.
8. Kim RJ, Fieno DS, Parrish TB, et al. Relationship of MRI delayed contrast enhancement to irreversible injury, infarct age, and contractile function. Circulation 1999;100:1992–2002.
9. Lardo AC, McVeigh ER, Jumrussirikul P, et al. Visualization and temporal/spatial characterization of cardiac radiofrequency ablation lesions using magnetic resonance imaging. Circulation 2000;102:698–705.
10. Rogers WJ Jr., Kramer CM, Geskin G, et al. Early contrast-enhanced MRI predicts late functional recovery after reperfused myocardial infarction. Circulation 1999;99:744–50.
11. van Dockum WG, ten Cate FJ, ten Berg JM, et al. Myocardial infarction after percutaneous transluminal septal myocardial ablation in hypertrophic obstructive cardiomyopathy: evaluation by contrast-enhanced magnetic resonance imaging. J Am Coll Cardiol 2004;43: 27–34.
12. Haines DE. The biophysiscs and pathophysiology of lesion formation during radiofrequency catheter ablation. In: Zipes DP, Jalife J, editors. Cardiac Electrophysiology. From Cell to Bedside. Philadelphia, PA: W.B. Saunders Company, 2003:1018–27.
13. Weinmann HJ, Laniado M, Mutzel W. Pharmacokinetics of Gd-DTPA/dimeglumine after intravenous injection into healthy volunteers. Physiol Chem Phys Med NMR 1984;16:167–72.
14. Bassingthwaighte JB, Goresky CA. Modeling in the analysis of solute and water exchange in the microvasculature. In: Renkin EM, Michel CC, Geiger SR, editors. Handbook of Physiology. Bethesda, MD: American Medical Society, 1984:549–626.
15. Tong CY, Prato FS, Wisenberg G, et al. Measurement of the extraction efficiency and distribution volume for Gd-DTPA in normal and diseased canine myocardium. Magn Reson Med 1993;30:337–46.
16. Saeed M, Wendland MF, Masui T, Higgins CB. Reperfused myocardial infarctions on T1- and susceptibility-enhanced MRI: evidence for loss of compartmentalization of contrast media. Magn Reson Med 1994;31:31–9.
17. Rehwald WG, Fieno DS, Chen EL, Kim RJ, Judd RM. Myocardial magnetic resonance imaging contrast agent concentrations after reversible and irreversible ischemic injury. Circulation 2002;105:224–9.
18. Rochitte CE, Lima JA, Bluemke DA, et al. Magnitude and time course of microvascular obstruction and tissue injury after acute myocardial infarction. Circulation 1998;98:1006–14.
19. Saeed M, Lund G, Wendland MF, Bremerich J, Weinmann H, Higgins CB. Magnetic resonance characterization of the peri-infarction zone of reperfused myocardial infarction with necrosis-specific and extracellular nonspecific contrast media. Circulation 2001; 103:871–6.
20. Sievers B, Brandts B, Moon JC, Pennell DJ, Trappe HJ. Cardiovascular magnetic resonance of iatrogenic ventricular scarring due to catheter ablation for left ventricular tachycardia. Int J Cardiol 2003; 91:249–50.
21. Djavan B, Zlotta AR, Susani M, et al. Transperineal radiofrequency interstitial tumor ablation of the prostate: correlation of magnetic

resonance imaging with histopathologic examination. Urology 1997;50:986–92.
22. Goldberg SN, Dupuy DE. Image-guided radiofrequency tumor ablation: challenges and opportunities—part I. J Vasc Interv Radiol 2001;12:1021–32.
23. Merkle EM, Boll DT, Boaz T, et al. MRI-guided radiofrequency thermal ablation of implanted VX2 liver tumors in a rabbit model: demonstration of feasibility at 0.2 T. Magn Reson Med 1999;42: 141–9.
24. Merkle EM, Haaga JR, Duerk JL, Jacobs GH, Brambs HJ, Lewin JS. MR imaging-guided radio-frequency thermal ablation in the pancreas in a porcine model with a modified clinical C-arm system. Radiology 1999;213:461–7.
25. Miao Y, Ni Y, Bosmans H, et al. Radiofrequency ablation for eradication of pulmonary tumor in rabbits. J Surg Res 2001;99:265–71.
26. Boaz TL, Lewin JS, Chung YC, Duerk JL, Clampitt ME, Haaga JR. MR monitoring of MR-guided radiofrequency thermal ablation of normal liver in an animal model. J Magn Reson Imaging 1998;8:64–9.
27. Merkle EM, Shonk JR, Zheng L, Duerk JL, Lewin JS. MR imaging-guided radiofrequency thermal ablation in the porcine brain at 0.2 T. Eur Radiol 2001;11:884–92.